Visualisation of turbulent structures in a centrifugal pump's volute using large eddy simulation.

ASIM, T., MISHRA, R. and NSOM, B.

2019

Visualisation of Turbulent Structures in a Centrifugal Pump's Volute using Large Eddy Simulation

T. ASIM[a], R.MISHRA[b], B. NSOM[c]

a. School of Engineering, Robert Gordon University, UK (t.asim@rgu.ac.uk)
b. School of Computing & Engineering, University of Huddersfield, UK (r.mishra@hud.ac.uk)
c. Université de Bretagne Occidentale, IUT de Brest, IRDL UMR CNRS 6027, France (blaise.nsom@univ-brest.fr)

Abstract :

Centrifugal pumps are an integral part of process and chemical industries around the globe. The flow within vaneless volutes of centrifugal pumps is highly turbulent and three-dimensional. Conventional flow modelling techniques are usually incapable of capturing these complex flow structures. Moreover, use of 2-equation turbulence models in Computational Fluid Dynamics (CFD) cannot resolve the turbulent flow structures in pump's volutes. Visualisation of these complex and turbulent flow structures is very important in order to design the volutes appropriately. In the present study, Large Eddy Simulation (LES) based turbulence modelling approach has been used to analyse the complex flow structures in the volute of a commercial centrifugal pump. LES is more accurate in resolving larger eddies, while smaller eddies are modelled. Hence, flow predictions using LES are more realistic. It has been noticed that the interaction between the impeller blades and the tongue gives rise to flow non-uniformities in the volute. These flow non-uniformities are caused by the generation and subsequent propagation of three-dimensional complex turbulent flow structures. These flow structures absorb energy from the flow, imparting considerable head losses.

Mots clefs : Large Eddy Simulation, Centrifugal Pump, Sliding Mesh, Blade-Tongue Interaction.

1 Introduction

Centrifugal pumps are commonly used in a number of fluids handling systems. The performance of centrifugal pumps is crucial to the overall efficiency of the system. Many modern techniques have been developed to analyse the performance of centrifugal pumps. Computational Fluid Dynamics (CFD) is one such technique where the flow structures within the centrifugal pumps can be monitored. However, there are a number of CFD based solvers available in the world. The choice of appropriate solver is utmost important for the accuracy of the numerically predicted flow fields within the pump. Byskov et al [1] and Pedersen et al [2] investigated the flow fields within the impeller of a centrifugal pump using numerical and experimental methodologies. Steady-State Reynolds Averaged Navier-

Stokes (RANS) and Large Eddy Simulation (LES) solvers have been used to numerically predict the flow structures within the centrifugal pump. It has been noticed that RANS based solvers are not capable of accurately predicting the flow structures within the pump. However, the LES predicted flow fields matched reasonably well with the experimental data.

Yulin et al [3] extended Byskov's work to investigate the Detached Eddy Simulation (DES) based flow field prediction. The authors have observed that the numerically predicted results are in closer agreement with the experimental data, based on DES solver. Meanwhile, significant differences with the steady-state modelling have been noticed. Unsteady complex flow phenomena within the volute of a centrifugal pump have been numerically investigated by Zhang et al [4]. The authors used LES based solver and have observed that the distinct peaks observed in the pressure build-up curve of the pump are closely associated with the positioning of the impeller blades. Unsteady vortical structures in the near-tongue region are greatly influenced by the relative orientation of the impeller blades with respect to the tongue, and the upstream effects of the tongue significantly affects the vorticity distribution on the blade pressure side. Furthermore, it has been stated that the rotor-stator interaction is dominated by the vortex shedding in the wake of the blade trailing edge and vortical structure's impingement on the tongue with subsequent cutting and distortion.

Guleren et al [5] have reported that out of the available RANS models, k-ω performs the best in predicting the flow features within a centrifugal pump; however, it is still inferior in performance than LES as it cannot clearly capture the vortical structures near the impeller exit and near-tongue regions. Investigations on pressure fluctuations within the volute of centrifugal pumps have been reported by many researchers, however, spatio-temporal variations of pressure within the different sections of the volute have not been investigated in detail. Hence, in the present study, spatio-temporal variations of pressure using LES based numerical approach has been used to investigate the complex flow features within a centrifugal pump.

2 Numerical Modelling of the Centrifugal Pump

The centrifugal pump that has been numerically modelled is FH32/200AH model from Perdrollo. The pump has five backward type impeller blades, having an impeller diameter of 215mm. The inlet and outlet sections of the pump have diameters of 50mm and 32mm respectively. Figure 1 depicts the numerical model of the centrifugal pump under consideration.

Figure 1. Numerical model of the pump.

Large Eddy Simulation (LES) has been used in the present study. LES is a numerical technique to solve transient turbulent flows. In this technique, the large flow scales are resolved while the smaller scales are numerically modelled. The large flow scales are more energetic, anisotropic in nature and are mostly dependent on the fluid, flow and geometric variables. The smaller flow scales are assumed to be isotropic and universal [6]. In order to differentiate between the larger and smaller flow scales, filtering operation is often employed. The filtered mass and momentum conservation equations are:

$$\frac{\partial \bar{u}_i}{\partial x_i} = 0 \tag{1}$$

$$\frac{\partial \bar{u}_i}{\partial t} + \frac{\partial \bar{u}_i \bar{u}_j}{\partial x_j} = -\frac{1}{\rho}\frac{\partial \bar{P}}{\partial x_i} + \frac{\partial}{\partial x_j}\left(\nu \frac{\partial \bar{u}_i \bar{u}_j}{\partial x_j}\right) - \frac{\partial \tau_{ij}^{sgs}}{\partial x_j} + \varepsilon_{i\,j3} 2\Omega \bar{u}_j \tag{2}$$

where $\varepsilon_{i\,j3}$ is the Levi-Civita's alternating tensor. The last term of the equation represents the Coriolis force. The centrifugal force is combined with the pressure, resulting in $\bar{P}$. $\tau_{i\,j}^{sgs}$ represents the subgrid scale (SGS) stresses modelled based on Bousinesq approach, i.e.:

$$\tau_{i\,j}^{sgs} - \frac{1}{3}\delta_{ij}\tau_{kk}^{sgs} = -2\nu_t \bar{S}_{ij} \tag{3}$$

where δ_{ij} is the Kronecker delta, $\bar{S}_{ij}$ is the resolved-scale strain rate tensor, and ν_t is the SGS eddy viscosity. The resolved-scale strain rate tensor is defined as:

$$\bar{S}_{ij} \equiv \frac{1}{2}\left(\frac{\partial \bar{u}_i}{\partial x_j} + \frac{\partial \bar{u}_j}{\partial x_i}\right) \tag{4}$$

In the present study, the SGS stresses are numerically modelled using the Wall Adapting Local Eddy Viscosity (WALE) model. This model takes into account both the effects of strain and rotational rates. The SGS eddy viscosity for the WALE model is defined as:

$$\nu_t = (C_\omega \Delta)^2 \frac{(S_{ij}{}^d S_{ij}{}^d)^{\frac{3}{2}}}{(S_{ij}S_{ij})^{\frac{5}{2}} + (S_{ij}{}^d S_{ij}{}^d)^{\frac{5}{4}}} \tag{5}$$

The SGS eddy viscosity drops to zero near the walls. This provides the correct near-wall behaviour by returning the correct wall asymptotic behaviour for wall bounded flows. In equation (5):

$$S_{ij}{}^d = \frac{1}{2}\left(\bar{g}_{ij}{}^2 + \bar{g}_{ji}{}^2\right) - \frac{1}{3}\delta_{ij}\bar{g}_{kk}{}^2 \tag{6}$$

where Δ is the cube root of the cell volume and the model coefficient (C_ω) is 0.1. $\bar{g}_{ij}$ represents the resolved-scale velocity gradient and is of the order of resolved-scale strain rate tensor. The aforementioned flow governing equations (continuity and Navier-Stokes) are solved using finite volume technique. The meshing in the flow domain is shown in figure 2. Considering the complexity of the impeller, unstructured tetrahedral mesh is employed with about 8 million mesh elements. This mesh has been shown to predict the complex flow phenomena within this type of centrifugal pump with reasonable accuracy [7].

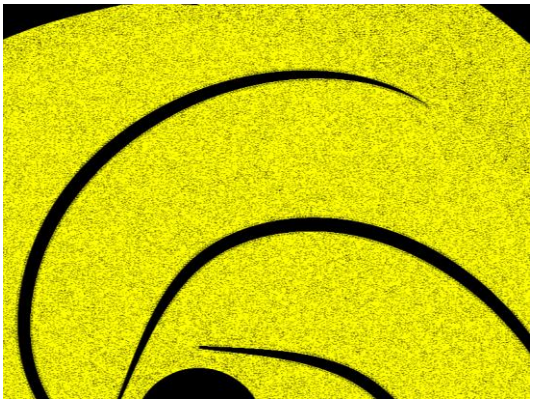

Figure 2. Meshing of the flow domain.

The working fluid in this study is water, with density and dynamic viscosity of 998.2kg/m^3 and 0.001003Pa-sec respectively. The inlet boundary condition has been specified as mass flow inlet of 12m^3/hr, while the outlet boundary condition specified is that of outflow. In order to rotate the impeller blades of the centrifugal pump, Sliding Mesh technique has been employed by dividing the computational domain into rotating and non-rotating zones. The impeller blades have been treated as a zone rotating at 2900rpm. No-slip condition has been specified on the walls of the flow domain. It has been assumed that the walls of the flow domain are hydrodynamically smooth. Furthermore, a time step size of 5.74713x10^{-5}sec has been specified in the present study, which corresponds to 1° rotation of the impeller blades per time step. It has been noticed that this time step size predicts the complex flow structures within the centrifugal pump with reasonable accuracy

3 Results and Discussions

The first step towards realistic evaluation of turbulent flow field within a flow domain is to obtain a statistically steady (or converged) solution. For this purpose, the solution was run for 3 revolutions of the impeller blades. The time history of the head developed by the centrifugal pump is shown in figure 3. It can be seen that the pump head becomes statistically steady after 1.5 revolutions (540°); hence, all the analysis carried out in the present study corresponds to the data obtained from the 3rd revolution of the centrifugal pump. Furthermore, it can be seen that the predicted head is in close agreement with the experimentally measured steady state head of the centrifugal pump at 12m^3/hr for ω=2900rpm, hence verifying the CFD results.

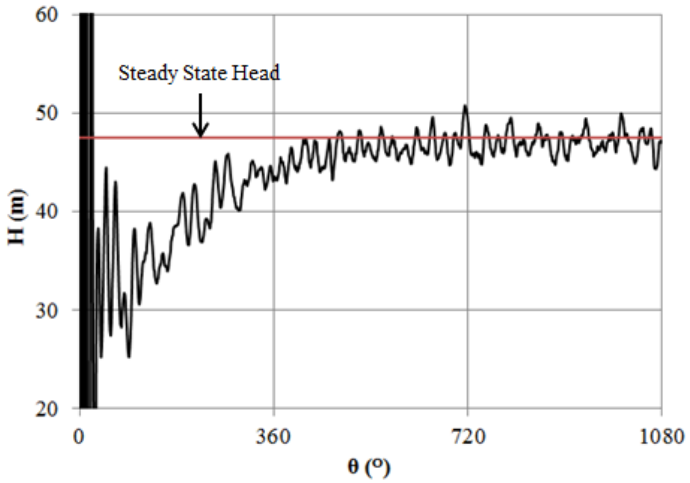

Figure 3. Time history of head developed by the pump.

Figure 4 depicts the variations in the head developed by the centrifugal pump in the 3rd revolution, as mentioned earlier. It can be seen that the head characteristics of the centrifugal pump are cyclic in nature, consisting of distinct positive and negative peaks, ranging between 44.3m and 50m of head. In order to carry out detailed investigations on the complex flow features, with respect to time, within the centrifugal pump in general, and in the volute in particular, comparisons have been drawn between the geometrical configurations at positive and negative peak geometrical configurations of the pump shown in figure 4. It has been observed that positive head peaks occur when the tongue region of the pump is in between two impeller blades, while the negative head peaks occur when an impeller blade is in-line with the tongue, as shown in figure 5.

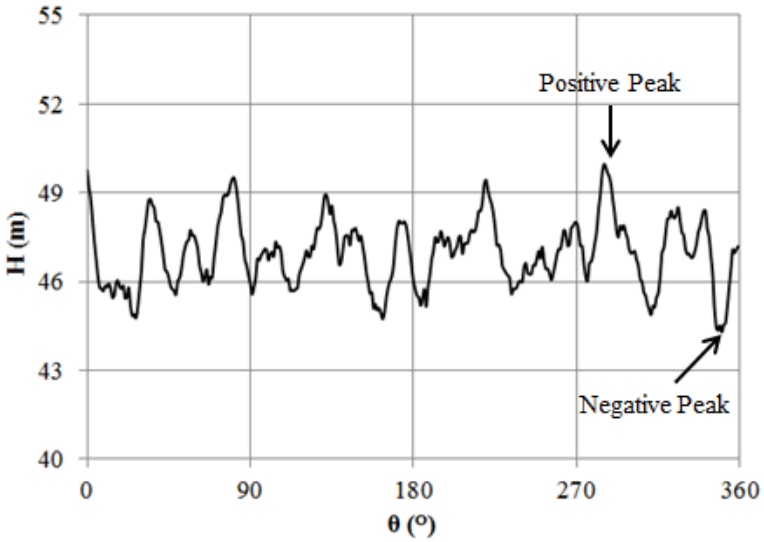

Figure 4. Variations of head with respect to angular position of the impeller blades.

Figure 5 depicts variations in the static gauge pressure within the impeller and volute region of the centrifugal pump at geometrical configurations corresponding to both the positive (left) and negative (right) peaks, as identified in figure 4. The scale of these variations has been kept constant for both these scenarios for effective comparison purposes. It can be seen that the pressure is generally negative in the vicinity of the impeller eye, causing suction effect. The pressure progressively builds up within the volute of the centrifugal pump as the kinetic energy imparted to the working fluid by the rotation of the impeller blades is converted into the pressure head. Hence, pressure is highest at the exit of the pump.

Further to the same general trend observed in both the geometrical configurations shown in figure 5, it can be seen that there are appreciable differences between the two pressure fields. For positive peak configuration (left), when the tongue is in-between two impeller blades, the pressure build-up within the volute, and downstream the tongue region, is significantly higher than for negative peak configuration (right). A closer look-up downstream the tongue region, as shown in figure 6, reveals that there exists a mixture of higher and lower pressure regions just downstream the tongue region.

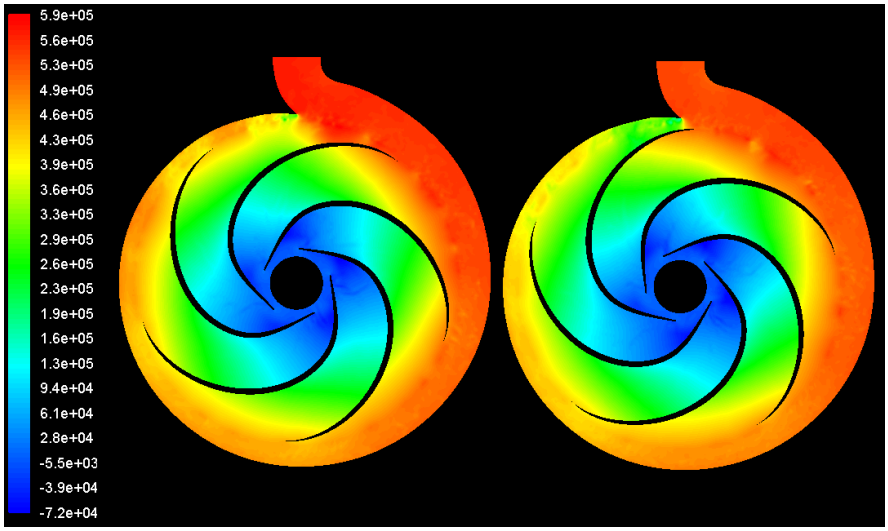

Figure 5. Variations of static gauge pressure (Pa) for positive and negative peak configurations.

In case of positive peak configuration, as the impeller blades are far from the tongue region, there is less restriction for the high pressure flow to enter the volute region. As the available area for the flow is more, the pressure is high (399kPa) whereas the velocity is low (12.4m/sec). Moreover, in case of negative peak configuration, as the impeller blade is in-line with the tongue, there is a restriction for the high pressure flow to enter the volute region. As the available area for the flow is reduced, the pressure is lower (301kPa) whereas the velocity is higher (14.5m/sec). Hence, at positive peak configurations, the effect of the tongue is less significant than at negative peak configurations.

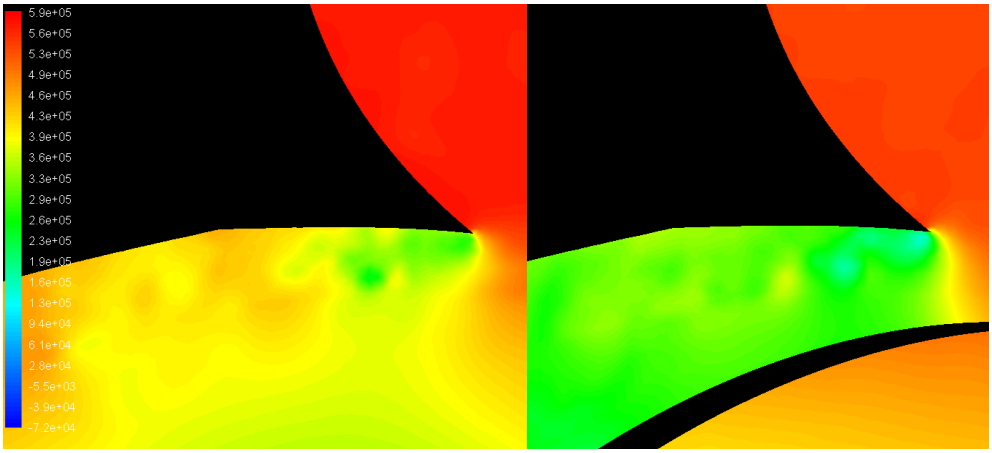

Figure 6. Variations of static gauge pressure (Pa) downstream the tongue region for positive and negative peak configurations.

Analysing the velocity magnitude vectors shown in figure 7, it can be further noticed that there are more and bigger recirculation zones downstream the tongue region in case of negative peaks configuration, while the flow is more uniform for positive peaks. This leads to higher losses in case of negative peaks due to the presence of intense secondary flows.

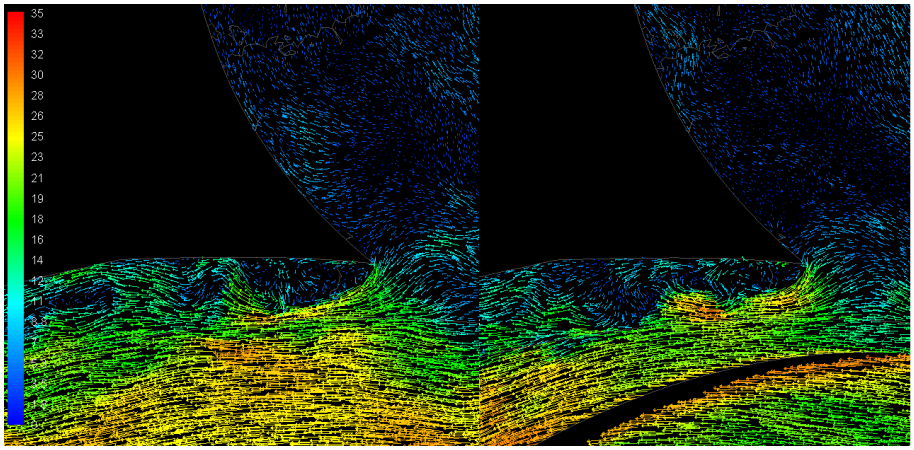

Figure 7. Velocity magnitude vectors (m/sec) in the vicinity of the tongue region for positive and negative peak configurations.

At this point, it becomes important to analyse these secondary flows in more detail. There are several methods for the detection of secondary flow structures, also known as vortical structures, where the method which is based on the velocity gradient tensor has been adopted in the present study. The vorticity and strain-rate tensors can be represented as:

$$\omega_{ij} = \frac{1}{2}\left(\frac{\partial u_i}{\partial x_j} - \frac{\partial u_j}{\partial x_i}\right) \tag{7}$$

$$SR_{ij} = \frac{1}{2}\left(\frac{\partial u_i}{\partial x_j} + \frac{\partial u_j}{\partial x_i}\right) \tag{8}$$

The velocity gradient tensor is:

$$D_{ij} = \omega_{ij} + SR_{ij} = \frac{\partial u_i}{\partial x_j} \tag{9}$$

The characteristic equation for the velocity gradient tensor is:

$$\lambda^3 + P\lambda^2 + Q\lambda + R = 0 \tag{10}$$

where P, Q and R are the three invariants of the velocity gradient tensor. The second invariant is known as Q-criterion, and can be represented as:

$$Q = \frac{1}{2}(\|\omega\|^2 - \|SR\|^2) \tag{11}$$

The Q-criterion defines vortex as a connected fluid region with a positive second invariant of the velocity gradient tensor i.e. Q > 0. This criterion also adds a secondary condition on the pressure, requiring it to be lower than the surrounding pressure in the vortex. A close examination of equation (11) reveals that it is the local balance between shear strain-rate and the vorticity magnitude, defining vortices as areas where the vorticity magnitude is greater than the strain-rate [8-9].

Figure 8 depicts the variations in the Q-criterion downstream the tongue region. The positive Q-criterion values correspond to higher vorticity magnitude than the shear strain-rate. It can be seen in the figure that vortical structures are formed downstream the tongue region, and their strength decreases as the distance from the tongue increases. Hence, vortical structures are most dominant in

the near tongue region. Furthermore, closely examining the figure reveals that for positive peak configuration (left) the significant vortical structures are limited to a small distance downstream the tongue, whereas for negative peak (right), these structures stretch farther downstream the tongue into the volute, and to some extent, into the impeller zone as well. The effective area occupied by these vortical structures is significantly higher for negative peaks configuration than for positive peaks, leading to increased losses.

In order to analyse the pressure developed by the centrifugal pump within the volute region, cross sectional planes were created at every 4.5° within the volute. Area-weighted average static gauge pressure by the centrifugal pump is computed on these planes. It has been verified that the pressure fluctuations are independent of the blade passage passing through the tongue region, as shown in figure 9. It can be seen that the pressure fluctuations within the volute of the centrifugal pump is cyclic in nature, with the number of peaks (either positive or negative) equal to the number of impeller blades (i.e. 5). Furthermore, it can also be seen that the amplitude of pressure fluctuations decreases as the cross-sectional area of the volute increases. Hence, the maximum amplitude of the pressure fluctuations is observed near the tongue region, while minimum near the exit of the centrifugal pump.

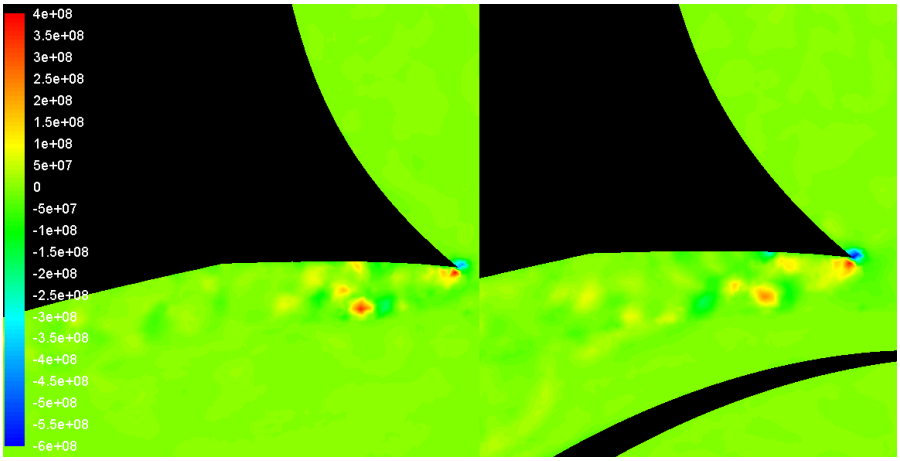

Figure 8. Q-criterion variations downstream the tongue region for positive and negative peak configurations.

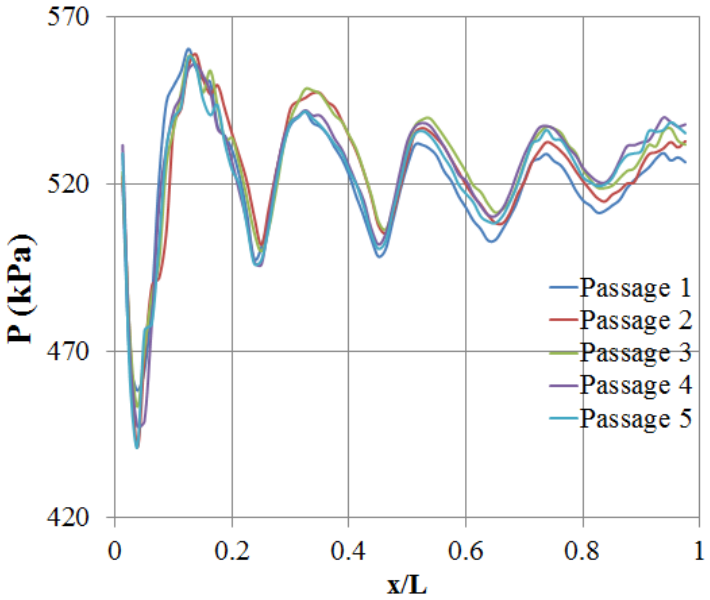

Figure 9. Variations in pressure fluctuations (kPa) within the volute for different blade passages.

Once it has been established that the blade passage has no significant effect on the pressure fluctuations, and that these fluctuations are dependent on the relative positioning of the impeller blades with respect to the tongue (for any given blade passage), it is important to critically analyse these pressure fluctuations in detail for a given blade passage. Figure 10 depicts the variations in the area-weighted average static gauge pressure within the volute for both positive and negative peak configurations. As mentioned earlier, just downstream the tongue region, the static pressure is significantly higher for positive peak configuration. Furthermore, the maximum amplitude of pressure fluctuations for positive and negative peak configurations are 102kPa and 96kPa respectively, which shows that the volute itself has limited contribution towards the pressure fluctuations, and these are largely dependent on the blade-tongue interactions.

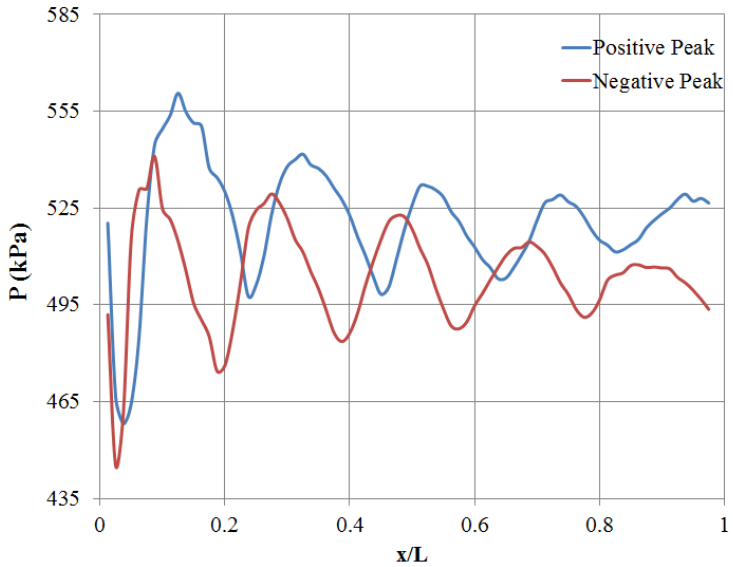

Figure 10. Variations in pressure fluctuations (kPa) within the volute for positive and negative peak configurations.

5 Conclusions

Unsteady flow field analysis within a centrifugal pump has been investigated in the present study using Large Eddy Simulation (LES) technique. It has been shown that LES predicts the complex flow features within a centrifugal pump with reasonable accuracy. Spatio-temporal pressure fluctuations have been analysed within the volute region, focusing on understanding the flow behaviour in the near-tongue region. It has been shown that the interaction of impeller blades with the tongue leads to complex secondary flow features i.e. vortices. The generation and subsequent dissipation of these vortical structures is strongly dependent on the geometrical orientation of the impeller blades with respect to the tongue. These flow structures are carried downstream the tongue, and are the primary reason behind cyclic nature of the head curve developed by the pump. The positive peaks of the head curve correspond to the orientation where the tongue is between two impeller blades, while the negative peaks correspond to tongue and impeller blades being in-line. The effective flow area available in the near tongue region is the primary cause of the build-up of these vortical structures. It can be further concluded that the volute itself has negligible effects on the pressure fluctuations within it.

Références

[1] R.K. Byskov, C.B. Jacobsen, N. Pedersen, Flow in a centrifugal pump impeller at design and off-design conditions: Part 2: Large Eddy Simulations, ASME Journal of Fluids Engineering125 (2003) 73-83

[2] N. Pedersen, P.S. Larsen, C.B. Jacobsen, Flow in a centrifugal pump impeller at design and off-design conditions: Part 1: Particle Image Velocimetry (PIV) and Laser Doppler Velocimetry (LDV) Measurements, ASME Journal of Fluids Engineering125 (2003) 61-72

[3] W. Yulin, L. Shuhong, S. Jie, Numerical Simulation on the Steady and Unsteady Internal Flows of a Centrifugal Pump, Numerical Simulations-Examples and Applications in Computational Fluid Dynamics, 2010

[4] N. Zhang, M. Yang, B. Gao, Z. Li, D. Ni, Investigation of Rotor-Stator Interaction and Flow Unsteadiness in a Low Specific Speed Centrifugal Pump, Journal of Mechanical Engineering62 (2016) 21-31

[5] K.M. Guleren, A. Turan, A. Pinarbasi, Large-eddy simulation of the flow in a low-speed centrifugal compressor, International Journal for Numerical Methods in Fluids56 (2008) 1271-1280

[6] W.J. Wang, Y.R. Cui, Y. Wang, G.D. Li, Q.H. Liang, G. Yin, Analysis on the blade inlet pressure fluctuation of the centrifugal pump based on LES, Proceedings of 6th International Conference on Pumps and Fans with Compressors and Wind Turbines, Beijing, China, 2013

[7] T. Asim, R. Mishra, Large Eddy Simulation based Analysis of Complex Flow Structures within the Volute of a Vaneless Centrifugal Pump, Sadhana42 (2017) 505-516

[8] V. Kolar Vortex Identification: New Requirements and Limitations, International Journal of Heat and Fluid Flow28 (2007) 638-652

[9] G. Haller, An Objective Definition of a Vortex, Journal of Fluid Mechanics525 (2005) 1-26